THE JOURNAL OF PHYSICAL CHEMISTRY C

Article

pubs.acs.org/JPCC

Signal-on Photoelectrochemical Aptasensor for Adenosine Triphosphate Detection Based on Sensitization Effect of CdS:Mn@Ru(bpy)$_2$(dcbpy) Nanocomposites

Gao-Chao Fan,[†] Ming Zhao,[†,§] Hua Zhu,[†] Jian-Jun Shi,[§] Jian-Rong Zhang,*[,†,‡] and Jun-Jie Zhu*[,†]

[†]State Key Laboratory of Analytical Chemistry for Life Science, Collaborative Innovation Center of Chemistry for Life Sciences, School of Chemistry and Chemical Engineering, Nanjing University, Nanjing 210093, China

[‡]School of Chemistry and Life Science, Nanjing University Jinling College, Nanjing 210089, China

[§]School of Chemical Engineering, Anhui University of Science and Technology, Huainan 232001, China

Supporting Information

ABSTRACT: A novel photoelectrochemical aptasensor for adenosine triphosphate (ATP) detection was developed by introducing inorganic−organic photoactive nanocomposites as sensitization agents to achieve significant signal amplification. Specifically, a TiO_2/Au hybrid structure was first fabricated by decorating Au nanoparticles on the surface of TiO_2 film, which then was used as the photoelectrochemical matrix for the immobilization of ATP aptamer probes; amino-functionalized CdS:Mn (CdS:Mn-NH_2) nanocrystals covalently bound with $Ru(bpy)_2(dcbpy)^{2+}$ (bpy = 2,2′-bipyridine; dcbpy = 2,2′-bipyridine-4,4′-dicarboxylic acid) to form CdS:Mn@Ru-(bpy)$_2$(dcbpy) photoactive nanocomposites, which were employed as signal amplification element labeling on the terminal of ATP aptamer probes. The ATP detection was performed via the photocurrent variation produced by the conformation change of ATP aptamer probes after specifically binding with ATP molecules. Before incubation with ATP, the ATP aptamer probe hybridized with its partly complementary DNA to form a rodlike double helix, which made the labeled sensitization agents of CdS:Mn@Ru(bpy)$_2$(dcbpy) far from the TiO_2/Au electrode surface, resulting in depressed sensitization effect. In the presence of ATP, the ATP aptamer probe specifically bound with ATP molecule to form a G-quadruplex structure, which made the CdS:Mn@Ru(bpy)$_2$(dcbpy) very close to the TiO_2/Au electrode surface, resulting in noticeably enhanced photocurrent intensity due to full activation of the sensitization effect. Accordingly, a signal-on photoelectrochemical aptasensor was constructed. The designed aptasensor exhibited a wide linear range from 0.5 pM to 5 nM with a low detection limit of 0.18 pM for ATP detection.

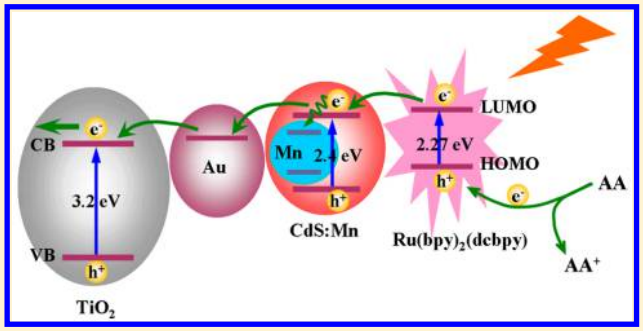

INTRODUCTION

Adenosine triphosphate (ATP) is a versatile nucleoside triphosphate, which is known as the major energy storage molecule within the cell and plays a vital role in regulation of cellular metabolism and biochemical pathways.[1,2] As a result, ATP levels can be utilized to assess cell viability, injury, proliferation, and inhibition induced by various biological agents or small molecule drugs.[3,4] In addition, ATP also serves as an important indicator of microbial contamination in the food industry.[5] Therefore, the accurate detection and quantification of ATP have become very important for biochemical study, clinical diagnosis, and food safety. For an extensive literature survey, the majority of reported strategies to detect ATP are based on the specific binding between ATP molecules and ATP aptamers. Since ATP aptamers were first selected by Huizenga et al. in 1995,[6] considerable efforts have been devoted to developing aptasensors for ATP detection by colorimetric,[7] fluorescent,[8] chemluminescence,[9] electrochemical,[10] and electrochemluminescence[11] methods. Despite the obvious merits of these methods, some of them involve the inadequacies of large background signal, evident sample volume, limited sensitivity, and high equipment cost.

Photoelectrochemical biosensing is a recently emerged yet vibrantly developing biosensor technique, which is based on the combination of photoelectrochemical process and specific biorecognition. Because it has the exciting features of simple equipment, low cost, easy miniaturization, low background signal, and high sensitivity,[12] photoelectrochemical biosensing has attracted growing interest and obtained a rapid development. To date, many different kinds of photoelectrochemical biosensors have been constructed and various target analytes such as DNA sequences, biomarkers, cancer cells, and other

Special Issue: Kohei Uosaki Festschrift

Received: August 20, 2015
Revised: September 25, 2015
Published: October 15, 2015

ACS Publications © 2015 American Chemical Society

DOI: 10.1021/acs.jpcc.5b08131
J. Phys. Chem. C 2016, 120, 15657−15665

Scheme 1. Fabrication Process of the Signal-on Photoelectrochemical Aptasensor toward ATP Detection

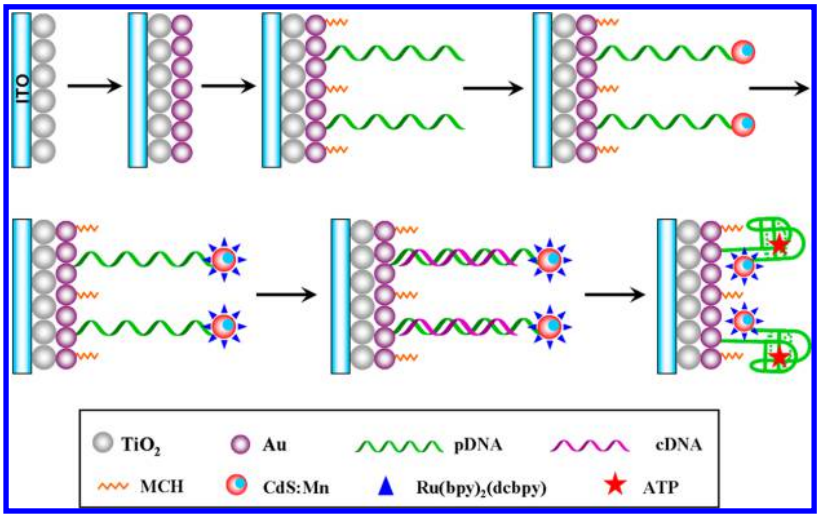

biomolecules have been successfully determined. Of course, the photoactive material and biorecognition probe are the two core components of each photoelectrochemical biosensor. Therefore, photoactive material plays a crucial role in its analytical performances. The photoactive materials applied in photoelectrochemical biosensing can be classified into inorganic and organic types. The inorganic photoactive materials mainly belong to semiconductor nanocrystals or quantum dots such as TiO_2,[13] ZnO,[14] CdS,[15] CdSe,[16] and CdTe,[17,18] whereas the organic photoactive materials are primarily attributed to small molecular dyes such as porphyrin,[19,20] phthalocyanine,[21] ruthenium complexes,[22,23] and carboxylated perylene.[24,25] For inorganic photoactive materials, they possess the advantages of high carrier mobility, large surface area, high extinction coefficient, as well as high quantum yield;[26−28] for organic photoactive materials, they have the advantages of high light-absorption efficiency, wide absorption range, and diverse electronic structure.[29−31] Because different types of photoactive materials have their unique merits, combining inorganic photoactive materials with organic types to form inorganic−organic composite structures can take full advantage of the merits of each and effectively promote the photocurrent conversion efficiency.[32−35] Thus, employing inorganic−organic photoactive composites as sensitization agents for signal amplification can contribute to an excellent sensitivity for photoelectrochemical detection. However, to the best of our knowledge, this excellent signal amplification strategy has not been reported in any of photoelectrochemical bioassays to date.

Herein, we present a novel signal-on photoelectrochemical aptasensor toward ATP detection based on the sensitization effect of inorganic−organic photoactive nanocomposites for signal amplification, as illustrated in Scheme 1. First, TiO_2 nanoparticles were covered on a bare indium−tin oxide (ITO) slice, and the compact film was formed after high-temperature calcination. Then Au nanoparticles were decorated onto the TiO_2 film to produce TiO_2/Au hybrid structure, and it was used as the photoelectrochemical matrix of the sensing electrode. After ATP aptamer probes (pDNA) were bound with the deposited Au nanoparticles through Au−S bond, the unbound sites on the electrode surface were blocked with 6-hydroxy-1-hexanethiol (MCH). Subsequently, CdS:Mn-NH_2 nanocrsytals were labeled on the terminal of pDNA via the linking of glutaraldehyde (GLD) molecules, and then multiple $Ru(bpy)_2(dcbpy)^{2+}$ dyes (the structural formula is shown in Figure S1) were bound on the surface of the anchored CdS:Mn-NH_2 nanocrsytals via the classic EDC coupling reaction. After partly complementary DNA (cDNA) hybridized with pDNA, the ATP molecules were detected by the photocurrent increase caused by conformation change of the pDNA from rodlike double helix to G-quadruplex structure, which resulted in full activation of the sensitization effect of CdS:Mn@$Ru(bpy)_2(dcbpy)$ photoactive nanocomposites. The designed photoelectrochemical aptasensor exhibited high sensitivity, satisfactory selectivity, reproducibility, and stability toward ATP detection.

EXPERIMENTAL SECTION

Materials and Reagents. ITO slices (type JH52, ITO coating 30 ± 5 nm, sheet resistance ≤10 Ω/square) were ordered from Nanjing Zhongjingkeyi Technology Co., Ltd. (China). TiO_2 powder (P25) was purchased from the Degussa Co. (Germany). Tris(2-carboxyethyl)phosphine (TCEP), chloroauric acid ($HAuCl_4·4H_2O$), 6-hydroxy-1-hexanethiol (MCH), *N*,*N*-dimethylformamide (DMF), cysteamine, Ru-$(bpy)_2(dcbpy)$ $(PF_6)_2$NHS, adenosine triphosphate (ATP), cytidine triphosphate (CTP), guanosine triphosphate (GTP), and uridine triphosphate (UTP) were all obtained from Sigma-Aldrich (US). Cadmium nitrate ($Cd(NO_3)_2·4H_2O$), manganese acetate ($Mn(Ac)_2·4H_2O$), sodium sulfide ($Na_2S·9H_2O$), and sodium hydroxide (NaOH) were purchased from Nanjing Chemical Reagent Co., Ltd. (China). Glutaraldehyde (GLD, 25% aqueous solution) and ascorbic acid (AA) were obtained from Sinopharm Chemical Reagent Co., Ltd. (China). All other reagents were of analytical grade and used as received. All aqueous solutions were prepared with deionized water (DI water, 18.2 MΩ/cm), which was obtained from a Milli-Q water purification system. Tris-HCl buffer solution (pH 7.4, 10 mM) containing 0.1 M NaCl was used for preparation and hybridization of DNA stock solutions.

The oligonucleotides were ordered from Shenggong Bioengineering Co., Ltd. (Shanghai, China) with the following sequences: ATP aptamer probe (pDNA), 5′-NH_2-$(CH_2)_6$-**ACC TGG GGG AGT ATT GCG GAG GAA GGT** CAT CAT CAT TTT-SH-3′; partly complementary DNA (cDNA), 5′-ACC TTC CTC CGC AAT ACT CCC CCA GGT-3′.

DOI: 10.1021/acs.jpcc.5b08131
J. Phys. Chem. C 2016, 120, 15657−15665

Apparatus. Photoelectrochemical measurements were performed with a homemade photoelectrochemical system. A 500 W Xe lamp was used as the irradiation source with the light intensity of 400 $\mu W \cdot cm^{-2}$ estimated by a radiometer (Photoelectric Instrument Factory of Beijing Normal University). Photocurrent was measured on a CHI 660D electrochemical workstation (Shanghai Chenhua Apparatus Corporation, China) with a three-electrode system: a modified ITO electrode with a geometrical area of 0.25 cm^2 as working electrode, a Pt wire as counter electrode, and a saturated Ag/AgCl electrode as reference electrode. The ultraviolet−visible (UV−vis) absorption spectra were tested on a UV-3600 UV−visible spectrophotometer (Shimadzu, Japan). ζ potential was tested on ZETASIZER nanoseries (Nano-ZS, Malvern, England). Transmission electron microscopy (TEM) was performed with a JEOL-2100 transmission electron microscope (JEOL, Japan). Field-emission scanning electron microscopy (FE-SEM) was carried out on a Hitachi S-4800 scanning electron microscope (Hitachi Co., Japan) equipped with EX-250 Energy-dispersive X-ray spectroscopy instrument (EDX, HORIBA Co., Japan). Electrochemical impedance spectroscopy (EIS) was performed on an Autolab potentiostat/galvanostat (PGSTAT 30, Eco Chemie B.V., Utrecht, Netherlands) with a three-electrode system in 0.1 M KCl solution containing 5.0 mM $K_3[Fe(CN)_6]/K_4[Fe(CN)_6]$ (1:1) mixture as a redox probe, and spectra were recorded in the frequency range of 0.01 Hz to 100 kHz with an amplitude of 5 mV.

Synthesis of CdS:Mn-NH_2 Nanocrystals. The bare CdS:Mn nanocrystals were synthesized based on a previously reported route.[36] Typically, 0.6 mmol of $Cd(NO_3)_2$ and 0.06 mmol of $Mn(Ac)_2$ were first mixed in 50 mL of DI water. After the mixture solution was heated to 70 °C under stirring, 10 mL of 0.05 M freshly prepared Na_2S solution was added; orange-yellow precipitates were instantly generated. The reaction was kept at 70 °C for 3 h with continuous stirring. The resulting precipitates were centrifuged and washed with absolute ethanol twice and DI water three times. The obtained precipitates were redispersed into DI water for collecting the upper yellow solution. To acquire amino-functionalized CdS:Mn nanocrystals, the collected upper yellow solution was first added by excessive amount of cysteamine aqueous solution, and then was incubated under shaking at room temperature for 6 h. Finally, the resulting solution was centrifuged by Millipore ultrafiltration centrifuge tube (molecular weight cutoff, 3000) several times, resulting in the desired CdS:Mn-NH_2 nanocrystals.

Preparation of ITO/TiO_2/Au Electrode. A 10 mg sample of TiO_2 powder was ultrasonically dispersed in 10 mL of DI water, and then 20 μL of this homogeneous suspension (1.0 mg/mL) was dropped onto a piece of ITO slice with fixed area of 0.25 cm^2. After being dried, the film was sintered at 450 °C in air for 30 min and then cooled to room temperature. The deposition of Au nanoparticles on ITO/TiO_2 electrode was similar to the literature method.[37] The TiO_2 modified electrode was first immersed into 0.01 M $HAuCl_4$ aqueous solution for 1 h. The pH of the solution was adjusted to 4.5 by dropwise addition of 0.2 M NaOH solution. Afterward, the electrode was washed with DI water thoroughly and dried in air, and then was annealed at 300 °C for 2 h in air atmosphere. Consequently, the desired ITO/TiO_2/Au electrode was obtained.

Fabrication of the Aptasensor. Initially, 20 μL of 2 μM ATP aptamer probe (pDNA) which was activated by TCEP (0.6 μL, 10 mM) for 1 h was dropped on the ITO/TiO_2/Au electrode, and it was allowed to incubate at 4 °C overnight. After being rinsed with Tris-HCl buffer (10 mM, pH 7.4) to remove the unbound pDNA, the electrode was blocked with 20 μL of 1 mM MCH at room temperature for 1 h followed by washing with Tris-HCl buffer. Subsequently, 20 μL of 5% GLD solution was dropped onto the electrode and remained at room temperature for 1 h. Then the electrode was rinsed with DI water thoroughly to remove physically adsorbed GLD. Next, 20 μL of CdS:Mn-NH_2 nanocrystals was dropped on the electrode and incubated at room temperature for 1 h. After being rinsed with DI water, the electrode was covered with 20 μL of DMF solution containing 1 mM $Ru(bpy)_2(dcbpy)$ $(PF_6)_2$NHS and incubated at room temperature for 6 h. The electrode was then rinsed with DI water to remove the excessive unbound dyes and incubated with 20 μL of 1 μM partly complementary DNA at 37 °C for 1 h, which allowed cDNA to hybridize with pDNA. After being rinsed with Tris-HCl buffer, the resulting electrode was incubated with 20 μL of different concentrations of ATP solutions at 37 °C for 1 h. Finally, the electrode was rinsed with Tris-HCl buffer and prepared for photoelectrochemical detection.

Photoelectrochemical Measurement. Photoelectrochemical detection was carried out at room temperature in Tris-HCl buffer solution (pH 7.4, 0.1 M) containing 0.1 M AA, which served as a sacrificial electron donor during the photocurrent measurement. White light produced by Xe lamp, with a spectral range of 200−2500 nm, was utilized as excitation light and was switched on and off every 10 s. The applied potential was 0.0 V. The AA electrolyte was deaerated by pure nitrogen for 15 min before photocurrent measurement.

RESULTS AND DISCUSSION

Photoelectrochemical Mechanism of the Aptasensor. Generally, the sensitivity of the photoelectrochemical bioassay depends on the extent of photocurrent change when target analytes were detected. Herein, inorganic−organic photoactive nanocomposites were employed as sensitization agents for signal amplification, and the photogenerated electron-transfer mechanism of the aptasensor is shown in Scheme 2. In this protocol, the TiO_2/Au hybrid structure acted as substrate photoactive material of the sensing electrode, whereas CdS:Mn@$Ru(bpy)_2(dcbpy)$ photoactive nanocomposites acted as the sensitization agents. TiO_2 is a wide energy band gap (~3.2 eV) semiconductor material, which can absorb only the ultraviolet light (<387 nm). However, it has been proven to be an excellent electrode material because of its good biocompatibility, high stability, low cost, and environmental

Scheme 2. Photogenerated Electron-Transfer Mechanism of the Aptasensor toward ATP Detection

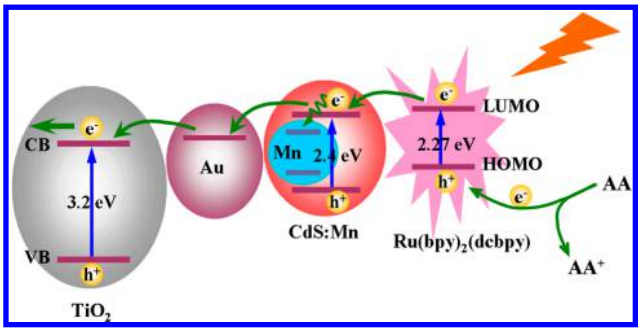

DOI: 10.1021/acs.jpcc.5b08131
J. Phys. Chem. C 2016, 120, 15657−15665

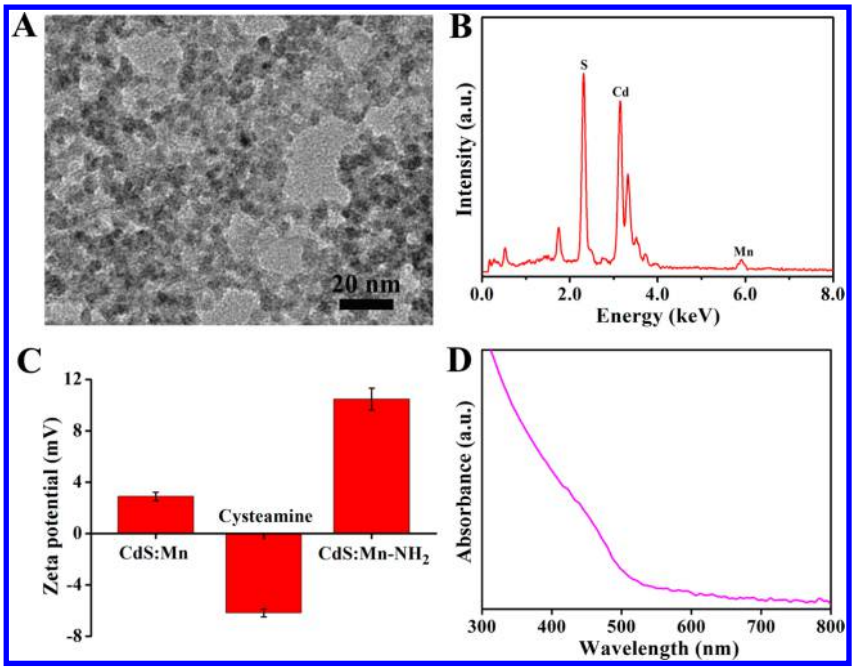

Figure 1. (A) TEM image and (B) EDX spectrum of the bare CdS:Mn nanocrystals; (C) ζ potentials of the bare CdS:Mn, cysteamine, and CdS:Mn-NH_2; (D) UV−vis absorption spectrum of the CdS:Mn-NH_2 nanocrystals.

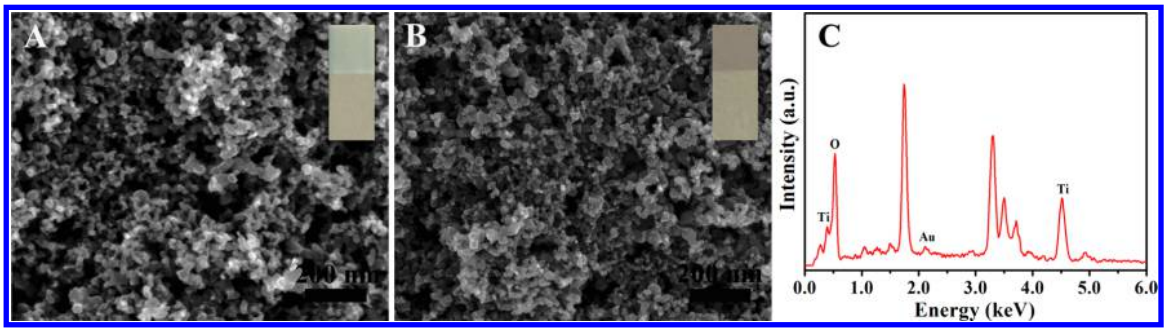

Figure 2. Typical SEM images of the (A) ITO/TiO_2 and (B) ITO/TiO_2/Au electrodes; (C) EDX spectrum of the ITO/TiO_2/Au electrode. Insets in parts A and B: photograph images of the corresponding electrodes.

safety. As an inorganic sensitization agent, CdS has a narrower energy band gap (~2.4 eV) and its absorption range can extend to the middle-wavelength light. In order to improve electron−hole recombination, Mn^{2+} was introduced into CdS to form CdS:Mn doping structure, because the lifetime of electron−hole recombination for CdS:Mn is up to microseconds, which is much longer than that of CdS, which is nanoseconds.[38] As a kind of dye, polypyridyl ruthenium complexes have been proven to be one of the most effective organic sensitization agents for solar cells to enhance the photocurrent conversion efficiency. $Ru(bpy)_2(dcbpy)^{2+}$ is a member of the polypyridyl ruthenium complexes, and its UV−vis absorption spectrum is shown in Figure S2. The optical band gap of $Ru(bpy)_2(dcbpy)^{2+}$ estimated from the band edge of absorption (~546 nm) was 2.27 eV. Because CdS:Mn nanocrystals possessed large surface area, more dyes of $Ru(bpy)_2(dcbpy)^{2+}$ were covalently bound on their surface to form CdS:Mn@$Ru(bpy)_2(dcbpy)$ inorganic−organic photoactive nanocomposites. The photoactive nanocomposites could evidently increase the absorption efficiency of the light energy, effectively inhibit the electron−hole recombination, and significantly promote the photocurrent response accordingly. The function of Au nanoparticles here was primarily to firmly bind with pDNA via Au−S bond. In addition, the Au nanoparticles could also act as light-scattering centers to increase the light absorption of the CdS:Mn@$Ru(bpy)_2(dcbpy)$ nanocomposites and further improve the sensitization effect.[39,40] The generation of sensitization effect was regulated by the conformation change of pDNA, because the electron transfer was a distance-dependent process. In the absence of ATP, the pDNA hybridized with its cDNA and formed a more rigid, rodlike double helix. At this time, the labeled CdS:Mn@$Ru(bpy)_2(dcbpy)$ nanocomposites were far from the TiO_2/Au electrode surface and the sensitization effect was depressed. While in the presence of the ATP, the pDNA released its cDNA and bound with ATP molecule to form a stable G-quadruplex structure. In this case, the labeled CdS:Mn@$Ru(bpy)_2(dcbpy)$ nanocomposites were very close to the TiO_2/Au electrode surface, resulting in evidently increased photocurrent intensity produced by full motivation of the sensitization effect. Accordingly, the target analytes of ATP molecules could be sensitively and specifically detected.

Characterization of CdS:Mn and CdS:Mn-NH_2 Nanocrystals. Panels A and B of Figure 1 show the TEM image and EDX spectrum of the bare CdS:Mn nanocrystals, respectively. According to the outline in the TEM image, the average size of the as-prepared bare CdS:Mn nanocrystals was evaluated to be

DOI: 10.1021/acs.jpcc.5b08131
J. Phys. Chem. C 2016, 120, 15657−15665

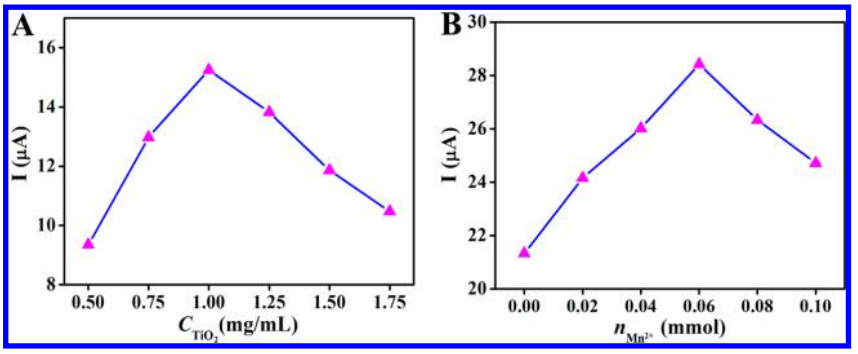

Figure 3. Effect of (A) TiO_2 concentration on photocurrent intensity of ITO/TiO_2/Au electrode and (B) mole amount of Mn^{2+} on photocurrent intensity of ITO/TiO_2/Au/pDNA/MCH/CdS:Mn electrode.

about 5 nm. In the EDX spectrum of CdS:Mn, elements Cd, S, and Mn are clearly observed. However, other elements such as Si, In, Sn, etc. came from the ITO substrate. As shown in Figure 1C, the initial ζ potential of the solution for bare CdS:Mn nanocrystals was a little positive (+2.9 mV) because the added amount of negatively charged S^{2-} was a little less than that of positively charged Cd^{2+} in the synthesis process; the ζ potential of the cysteamine solution was obviously negative (−6.2 mV) because electronegativity of the sulfhydryl group in cysteamine was stronger than electropositivity of the amino group. However, the ζ potential became evidently positive (+10.5 mV) for the solution of CdS:Mn-NH_2 nanocrystals, because the sulfhydryl group in cysteamine had reacted with Cd^{2+} on the surface of bare CdS:Mn to form Cd−S bond, leading to positively charged amino group on the surface of CdS:Mn nanocrystals. Figure 1D displays the UV−vis absorption spectrum of CdS:Mn-NH_2 nanocrystals. It exhibited a broad absorption range below 530 nm, but without any evident absorption peak.

Characterization of ITO/TiO_2/Au Electrode. Panels A and B of Figure 2 exhibit the SEM images of the ITO/TiO_2 and ITO/TiO_2/Au electrodes, respectively. After the TiO_2 film was formed on ITO electrode, a large number of TiO_2 nanoparticles (with the size range of 22−28 nm) as well as pores could be clearly observed, as shown in Figure 2A. After Au subsequently grew on the TiO_2 modified electrode, it could be seen (Figure 2B) that many relatively small particles with the average size of about 8 ± 2 nm were decorated on the TiO_2 film, and the pore size evidently decreased. In addition, the insets in panels A and B of Figure 2 show the photograph images of ITO/TiO_2 and ITO/TiO_2/Au electrodes, respectively. According to color changes from white to violet of the electrode surfaces, it also suggested the successful preparation of ITO/TiO_2/Au electrode. Figure 2C shows the EDX spectrum of the ITO/TiO_2/Au electrode. TiO_2/Au indicator elements of Ti, O, and Au are observed in the spectrum. Among which other elements of Si, In, Sn, etc. were from the ITO slice. In addition, elemental mapping analysis of TiO_2/Au suggested the presence of Ti, O, and Au components in the hybrid (Figure S3), and the deposited Au element was well scattered on the TiO_2 film.

Optimal Conditions of the Aptasensor Preparation. To obtain optimal thickness of the TiO_2 film, different concentrations of TiO_2 suspension were used to prepare ITO/TiO_2/Au electrode; other conditions were fixed. As displayed in Figure 3A, the ITO/TiO_2/Au electrode fabricated with 1.0 mg/mL suspension exhibited the highest photocurrent intensity. Increasing the concentration of TiO_2 suspension could offer more TiO_2, resulting in more ultraviolet light absorption and increased photocurrent intensity. However, with further increasing the concentration of TiO_2 suspension, more surface recombination centers formed on the excessive TiO_2 and the diffusion resistance for electron motion in thicker TiO_2 film evidently increased,[41] which led to the gradual decrease in photocurrent intensity. Hence, a 1.0 mg/mL TiO_2 suspension was adopted for fabricating the electrode in the following experiments.

The doping ratio of Mn^{2+} in CdS:Mn-NH_2 nanocrystals could be adjusted by the addition of Mn^{2+} during the synthetic process of the bare CdS:Mn nanocrystals. Figure 3B displays the photocurrent intensity of the ITO/TiO_2/Au/pDNA/MCH/CdS:Mn electrodes prepared with different mole amounts of Mn^{2+} and with other conditions fixed. Along with the addition of Mn^{2+}, the doping ratio would increase.[42] At this time, more electronic states were created in the middle band gap of CdS, resulting in significantly reduced electron−hole recombination, and the photocurrent intensity increased. As could be observed, the electrode fabricated with 0.06 mmol of Mn^{2+} possessed the optimal photocurrent intensity. After further increases in the mole amount of Mn^{2+}, more and more excitation electrons were trapped by excess Mn−Mn ion pairs,[43] leading to the decrease of photocurrent intensity. Thus, 0.06 mmol of Mn^{2+} was used to synthesize the CdS:Mn-NH_2 nanocrystals.

EIS Characterization of the Aptasensor Fabrication. As a useful tool for characterizing the interface properties of electrodes, electrochemical impedance spectroscopy was utilized to monitor the construction process of the aptasensor. Figure 4 exhibits the impedance spectra of the electrodes

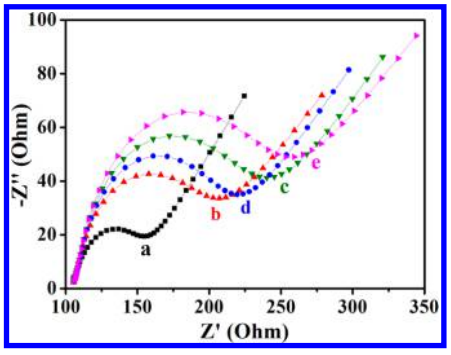

Figure 4. EIS of (a) the ITO/TiO_2/Au electrode, (b) after pDNA and MCH immobilization, (c) after anchoring CdS:Mn-NH_2 nanocrystals, (d) after further anchoring $Ru(bpy)_2(dcbpy)^{2+}$ dyes, and (e) after cDNA hybridization.

DOI: 10.1021/acs.jpcc.5b08131
J. Phys. Chem. C 2016, 120, 15657−15665

formed in different fabrication steps. Each impedance spectrum consists of a semicircle reflecting the electron-transfer limited process and a linear part originating from the diffusion limited process. The electron-transfer resistance (R_{et}) equals the semicircle diameter, which indicates the restricted diffusion of the redox probe accessing the layer. For ITO/TiO_2/Au electrode, the impedance spectrum exhibited a small R_{et} (curve a). After pDNA and MCH immobilization, the R_{et} increased because of low conductivity of DNA sequences and MCH molecules (curve b). After anchoring of CdS:Mn-NH_2 nanocrystals, the R_{et} increased (curve c). This was because the poor conductivity of both the CdS:Mn semiconductor and GLD bridging molecules played a major role, although amino groups on CdS:Mn-NH_2 nanocrystals generated a positively charged surface that improved the ability of the negatively charged redox probe $[Fe(CN)_6]^{3-/4-}$ to access the electrode surface. After further anchoring of $Ru(bpy)_2(dcbpy)^{2+}$ dyes, the R_{et} moderately decreased (curve d). That was because the anchoring of one $Ru(bpy)_2(dcbpy)^{2+}$ cationic dye could consume two amino groups and the electropositivity of one $Ru(bpy)_2(dcbpy)^{2+}$ dye was stronger than that of two amino groups. After the electrode was incubated with cDNA, the R_{et} evidently increased (curve e), indicating that the cDNA had hybridized with pDNA. Thus, the EIS characterization suggested the designed aptasensor was successfully fabricated.

Photocurrent Characterization of the Aptasensor Fabrication. The fabrication process of the aptasensor could also be monitored by photocurrent responses, as shown in Figure 5. The ITO/TiO_2/Au electrode exhibited a relatively small photocurrent intensity (curve a). It was because that TiO_2 can absorb only the ultraviolet light resulting in low photocurrent conversion efficiency. Meanwhile, as the Fermi level of Au was lower than that of TiO_2, the photogenerated electrons in TiO_2 could partly injected in Au nanoparticles to equilibrate the Fermi levels between them, resulting in further decreased photocurrent intensity.[44,45] It was worth noting that the photocurrent intensity moderately increased after pDNA and MCH immobilization (curve b), although both the pDNA sequences and MCH molecules possessed weak charge-transfer abilities. This might be because the immobilization of pDNA and MCH had weakened the Fermi-level alignment of TiO_2/Au hybrid structure. After CdS:Mn-NH_2 nanocrystals and Ru-$(bpy)_2(dcbpy)^{2+}$ dyes were successively anchored on the terminal of pDNA, the photocurrent intensity gradually increased (curve c and curve d). Yet, the photocurrent increments were not that obvious, because the pDNA was in a flexible single-strand form leading to partly generated sensitization effect. After cDNA hybridized with pDNA, the photocurrent intensity decreased (curve e). It was mainly because that the pDNA changed from flexible single-strand structure into more rigid, rodlike double helix, which forced the anchored CdS:Mn@$Ru(bpy)_2(dcbpy)$ nanocomposites further far away from the electrode surface, leading to greatly depressed sensitization effect. While the prepared sensing electrode was incubated with 20 μL of 100 nM ATP, the photocurrent intensity increased remarkably (curve f). This was mainly because that the pDNA had specifically bound with ATP molecule and formed a stable G-quadruplex structure, which caused the anchored CdS:Mn@$Ru(bpy)_2(dcbpy)$ nanocomposites very closed to the electrode surface, resulting in full activation of the sensitization effect. Meanwhile, as a type of small molecule, ATP possessed very small steric hindrance, and the photocurrent decrease for ATP immobilization was negligible. Therefore, the photocurrent responses proved the successful fabrication of the proposed aptasensor.

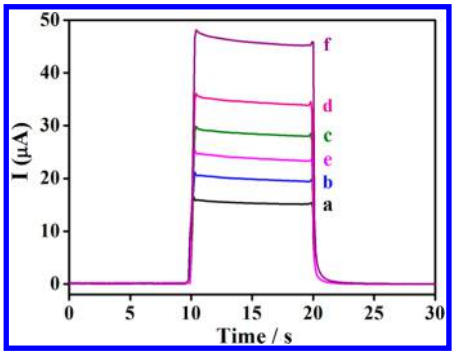

Figure 5. Photocurrent responses of (a) the ITO/TiO_2/Au electrode, (b) after pDNA and MCH immobilization, (c) after anchoring CdS:Mn-NH_2 nanocrystals, (d) after further anchoring Ru-$(bpy)_2(dcbpy)^{2+}$ dyes, (e) after cDNA hybridization, and (f) after incubation with 20 μL of 100 nM ATP.

Photoelectrochemical Detection toward ATP. The photoelectrochemical ATP detection was based on the conformation change of ATP aptamer probe from rodlike double helix to G-quadruplex structure after it specifically bound with ATP. The photocurrent response was directly related to the concentration of ATP. Figure 6A displays the photocurrent responses of the designed aptasensor after being incubated with different concentrations of ATP. As the sensitization effect could be fully generated in the presence of ATP, the photocurrent response gradually increased with elevating the ATP concentration. As shown in Figure 6B, the

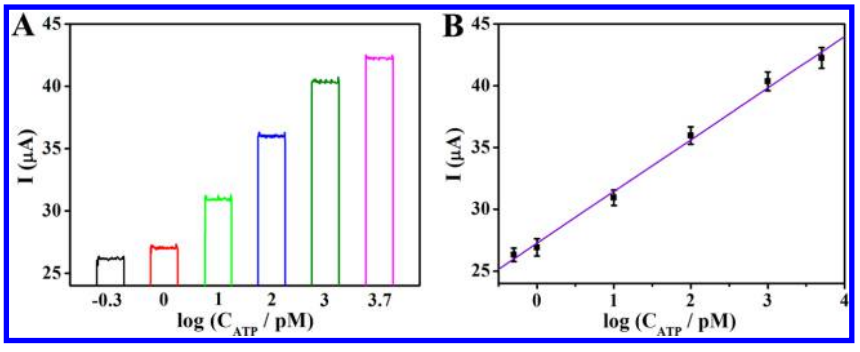

Figure 6. (A) Photocurrent response and (B) calibration curve of the aptasensor for the detection of different concentrations of ATP from 0.5 pM to 5 nM. The error bars show the standard deviation of five replicate determinations.

DOI: 10.1021/acs.jpcc.5b08131
J. Phys. Chem. C 2016, 120, 15657−15665

photocurrent response linearly increased with the increase of logarithm of ATP concentration in the range from 0.5 pM to 5 nM. The regression equation was $I = 27.25 + 4.19 \log C$ (pM), with a correlation coefficient of 0.9971. The detection limit (S/N = 3) for ATP concentration was estimated to be 0.18 pM (the calculation procedure for the detection limit is described in Supporting Information), which was evidently lower than that of recently reported, highly sensitive methods such as $Ru(bpy)_2dppz^{2+}$ sensitization-based photoelectrochemical biosensor (3.2 nM),[46] square wave voltammetry-based electrochemical assay (20 pM),[47] electrochemiluminescent biosensor (200 pM),[48] differential pulse stripping voltammetry-based electrochemical assay (100 pM),[49] loop DNA probe-based fluorescence strategy (1.2 pM),[50] etc. Moreover, in order to demonstrate the excellent performance of the sensitization effect of CdS:Mn@$Ru(bpy)_2$(dcbpy) nanocomposites, the aptasensor employing only CdS:Mn-NH_2 nanocrystals as sensitization agents for signal amplification was fabricated. The photoelectrochemical detection results revealed that the latter aptasensor with only CdS:Mn-NH_2 nanocrystals as sensitization agents exhibited a detection limit of 2.6 pM, which was 14 times higher than that of the former aptasensor. Hence, the control experiment also indicated an apparent superiority of the sensitization effect of CdS:Mn@$Ru(bpy)_2$(dcbpy) nanocomposites.

Specificity, Reproducibility, and Stability of the Aptasensor. The specificity of the designed aptasensor was evaluated by comparing the photocurrent response to some representative interferents, including cytosine triphosphate (CTP), guanosine triphosphate (GTP), and uridine triphosphate (UTP). It can be observed in Figure 7 that the

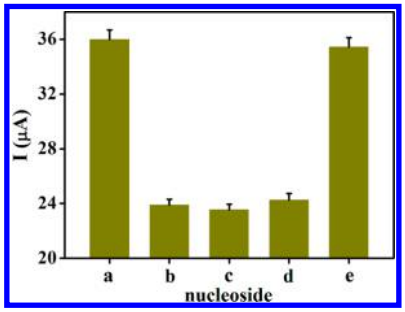

Figure 7. Photocurrent responses of the aptasensor to (a) 100 pM ATP, 1 nM (b) CTP, (c) GTP, (d) UTP, and (f) all of their mixture. The error bars show the standard deviation of five replicate determinations.

photocurrent responses to 1 nM CTP, GTP, and UTP were much lower than that of 100 pM of ATP, indicating negligible interference of these interferents. In addition, the photocurrent response to the mixed sample composed of 100 pM ATP, and 1 nM CTP, GTP, and UTP was also investigated, and no significant difference of photocurrent response could be observed as compared to the result obtained in the presence of only 100 pM ATP. All these results demonstrated that the proposed aptasensor had a satisfactory specificity toward ATP detection.

The reproducibility of the aptasensor was assessed by testing five independently fabricated sensing electrodes after being incubated with the same concentration of ATP solution. The photocurrent response offered relative standard deviations (RSDs) of 4.6% and 3.8% to 1 pM and 10 pM ATP detection, respectively, which suggested an acceptable reproducibility of this aptasensor.

The stability of the aptasensor was evaluated by the photocurrent change. After the sensing electrode was stored in a dark and humid environment at 4 °C for 2 weeks, the photocurrent intensity still maintained 92.4% of its initial response, indicating good storage stability. Additionally, the stability of the aptasensor was also estimated under different pH conditions. As displayed in Figure 8, the photocurrent

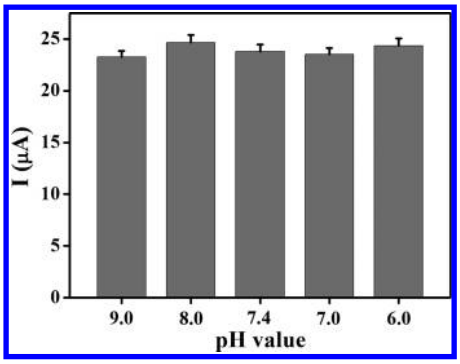

Figure 8. Photocurrent responses of the ATP aptasensor after being incubated in Tris-HCl buffer with varied pH from 9.0 to 6.0. The error bars show the standard deviation of five replicate determinations.

intensity of the aptasensor did not change after being incubated in Tris-HCl buffer with the variation of pH from 9.0 to 6.0, demonstrating good pH stability of the designed aptasensor.

Preliminary Application of the Aptasensor. The designed aptasensor was further applied to detect ATP molecules in human serum samples. The recoveries of ATP were used to evaluate its feasibility. From the analytical results presented in Table 1, it could be obtained that the recoveries of

Table 1. Detection of ATP in Human Serum Samples

no.	added (nM)	found (nM)	RSD (%)	recovery (%)
1	0.05	0.0462	5.3	92.4
2	0.2	0.2135	4.8	106.8
3	1	0.9750	4.1	97.5

three samples for the added ATP with 0.05, 0.2, and 1 nM were 92.4%, 106.8%, and 97.5%, respectively, which indicated that the proposed aptasensor has a promising potential for real sample applications.

CONCLUSIONS

In summary, the sensitization effect of inorganic−organic photoactive nanocomposites was first introduced into photoelectrochemical bioassay for signal amplification. The developed signal-on photoelectrochemical aptasensor was applied for the detection of ATP molecules. Based on the conformation change of ATP aptamer probes from rodlike double helix to G-quadruplex structure after specifically bound with ATP molecules, the activation of sensitization effect could be regulated. As sensitization agents, CdS:Mn@$Ru(bpy)_2$(dcbpy) photoactive nanocomposites could evidently increase the photocurrent signal when ATP molecules were detected. Due to excellent photoelectrochemical performances, the well-fabricated aptasensor exhibited a low detection limit of 0.18 pM for ATP detection. Moreover, because of its sensitivity, simplicity, specificity, reproducibility, and stability, the

DOI: 10.1021/acs.jpcc.5b08131
J. Phys. Chem. C 2016, 120, 15657−15665

proposed robust sensing strategy also can be extended to detect other important biomolecules and has a wide potential application in bioanalysis.

■ ASSOCIATED CONTENT

Supporting Information

The Supporting Information is available free of charge on the ACS Publications website at DOI: 10.1021/acs.jpcc.5b08131.

Structural formula (Figure S1) and UV−vis absorption spectrum (Figure S2) of the $Ru(bpy)_2(dcbpy)^{2+}$ dyes, elemental mapping analysis of TiO_2/Au hybrid structure (Figure S3), and calculation procedure for the detection limit (PDF)

■ AUTHOR INFORMATION

Corresponding Authors

*E-mail: jrzhang@nju.edu.cn.

*E-mail: jjzhu@nju.edu.cn.

Notes

The authors declare no competing financial interest.

■ ACKNOWLEDGMENTS

We gratefully appreciate the support from National Natural Science Foundation (21375059, 21175065, and 21335004) and the National Basic Research Program (2011CB933502) of China.

■ REFERENCES

(1) Abraham, E. H.; Okunieff, P.; Scala, S.; Vos, P.; Oosterveld, M. J. S.; Chen, A. Y.; Shrivastav, B.; Guidotti, G. Cystic Fibrosis Transmembrane Conductance Regulator and Adenosine Triphosphate. *Science* **1997**, *275*, 1324−1326.

(2) Atkinson, D. E.; Walton, G. M. Adenosine Triphosphate Conservation in Metabolic Regulation—Rat Liver Citrate Cleavage Enzyme. *J. Biol. Chem.* **1967**, *242*, 3239−3241.

(3) Verstraeten, L. M.; De Coninck, K.; Vlassak, K.; Verstraete, W.; Van de Werf, H.; Ilaiwi, M. ATP Content of Soils Estimated by Two Contrasting Extraction Methods. *Soil Biol. Biochem.* **1983**, *15*, 397−402.

(4) Lundin, A.; Hasenson, M.; Persson, J.; Pousette, A. Estimation of Biomass in Growing Cell-Lines by Adenosine-Triphosphate Assay. *Methods Enzymol.* **1986**, *133*, 27−42.

(5) Davidson, C. A.; Griffith, C. J.; Peters, A. C.; Fielding, L. M. Evaluation of Two Methods for Monitoring Surface Cleanliness—ATP Bioluminescence and Traditional Hygiene Swabbing. *Luminescence* **1999**, *14*, 33−38.

(6) Huizenga, D. E.; Szostak, J. W. A DNA Aptamer that Binds Adenosine and ATP. *Biochemistry* **1995**, *34*, 656−665.

(7) Wang, J.; Wang, L.; Liu, X.; Liang, Z.; Song, S.; Li, W.; Li, G.; Fan, C. A Gold Nanoparticle-Based Aptamer Target Binding Readout for ATP Assay. *Adv. Mater.* **2007**, *19*, 3943−3946.

(8) Xu, W.; Lu, Y. Label-Free Fluorescent Aptamer Sensor Based on Regulation of Malachite Green Fluorescence. *Anal. Chem.* **2010**, *82*, 574−578.

(9) Zhang, S. S.; Yan, Y. M.; Bi, S. Design of Molecular Beacons as Signaling Probes for Adenosine Triphosphate Detection in Cancer Cells Based on Chemiluminescence Resonance Energy Transfer. *Anal. Chem.* **2009**, *81*, 8695−8701.

(10) Zuo, X.; Xiao, Y.; Plaxco, K. W. High Specificity, Electrochemical Sandwich Assays Based on Single Aptamer Sequences and Suitable for the Direct Detection of Small-Molecule Targets in Blood and Other Complex Matrices. *J. Am. Chem. Soc.* **2009**, *131*, 6944−6945.

(11) Yao, W.; Wang, L.; Wang, H. Y.; Zhang, X. L.; Li, L. An Aptamer-Based Electrochemiluminescent Biosensor for ATP Detection. *Biosens. Bioelectron.* **2009**, *24*, 3269−3274.

(12) Liang, M. M.; Liu, S. L.; Wei, M. Y.; Guo, L. H. Photoelectrochemical Oxidation of DNA by Ruthenium Tris-(bipyridine) on a Tin Oxide Nanoparticle Electrode. *Anal. Chem.* **2006**, *78*, 621−623.

(13) An, Y. R.; Tang, L. L.; Jiang, X. L.; Chen, H.; Yang, M. C.; Jin, L. T.; Zhang, S. P.; Wang, C. G.; Zhang, W. A Photoelectrochemical Immunosensor Based on Au-Doped TiO_2 Nanotube Arrays for the Detection of α-Synuclein. *Chem. - Eur. J.* **2010**, *16*, 14439−14446.

(14) Tu, W. W.; Lei, J. P.; Wang, P.; Ju, H. X. Photoelectrochemistry of Free-Base-Porphyrin-Functionalized Zinc Oxide Nanoparticles and Their Applications in Biosensing. *Chem. - Eur. J.* **2011**, *17*, 9440−9447.

(15) Willner, I.; Patolsky, F.; Wasserman, J. Photoelectrochemistry with Controlled DNA-Cross-Linked CdS Nanoparticle Arrays. *Angew. Chem., Int. Ed.* **2001**, *40*, 1861−1864.

(16) Fan, G. C.; Ren, X. L.; Zhu, C.; Zhang, J. R.; Zhu, J. J. A New Signal Amplification Strategy of Photoelectrochemical Immunoassay for Highly Sensitive Interleukin-6 Detection Based on TiO_2/CdS/CdSe Dual Co-sensitized Structure. *Biosens. Bioelectron.* **2014**, *59*, 45−53.

(17) Fan, G. C.; Han, L.; Zhang, J. R.; Zhu, J. J. Enhanced Photoelectrochemical Strategy for Ultrasensitive DNA Detection Based on Two Different Sizes of CdTe Quantum Dots Cosensitized TiO_2/CdS:Mn Hybrid Structure. *Anal. Chem.* **2014**, *86*, 10877−10884.

(18) Fan, G.-C.; Han, L.; Zhu, H.; Zhang, J.-R.; Zhu, J.-J. Ultrasensitive Photoelectrochemical Immunoassay for Matrix Metalloproteinase-2 Detection Based on CdS:Mn/CdTe Cosensitized TiO_2 Nanotubes and Signal Amplification of SiO_2@Ab_2 Conjugates. *Anal. Chem.* **2014**, *86*, 12398−12405.

(19) Tu, W. W.; Dong, Y. T.; Lei, J. P.; Ju, H. X. Low-Potential Photoelectrochemical Biosensing Using Porphyrin-Functionalized TiO_2 Nanoparticles. *Anal. Chem.* **2010**, *82*, 8711−8716.

(20) Hu, Y. Q.; Xue, Z. H.; He, H. X.; Ai, R. X.; Liu, X. H.; Lu, X. Q. Photoelectrochemical Sensing for Hydroquinone Based on Porphyrin-Functionalized Au Nanoparticles on Graphene. *Biosens. Bioelectron.* **2013**, *47*, 45−49.

(21) Li, Y. J.; Ma, M. J.; Yin, G.; Kong, Y.; Zhu, J. J. Phthalocyanine-Sensitized Graphene-CdS Nanocomposites: An Enhanced Photoelectrochemical Immunosensing Platform. *Chem. - Eur. J.* **2013**, *19*, 4496−4505.

(22) Zhang, B. T.; Guo, L. H. Highly Sensitive and Selective Photoelectrochemical DNA Sensor for the Detection of Hg^{2+} in Aqueous Solutions. *Biosens. Bioelectron.* **2012**, *37*, 112−115.

(23) Zhang, X. R.; Xu, Y. P.; Zhao, Y. Q.; Song, W. L. A New Photoelectrochemical Biosensors Based on DNA Conformational Changes and Isothermal Circular Strand-Displacement Polymerization Reaction. *Biosens. Bioelectron.* **2013**, *39*, 338−341.

(24) Li, H. B.; Li, J.; Xu, Q.; Yang, Z. J.; Hu, X. Y. A Derivative Photoelectrochemical Sensing Platform for 4-nitrophenolate Contained Organophosphates Pesticide Based on Carboxylated Perylene Sensitized Nano-TiO_2. *Anal. Chim. Acta* **2013**, *766*, 47−52.

(25) Li, H. B.; Xue, Y.; Wang, W. Femtomole Level Photoelectrochemical Aptasensing for Mercury Ions Using Quercetin-Copper(II) Complex as the DNA Intercalator. *Biosens. Bioelectron.* **2014**, *54*, 317−322.

(26) Lee, Y. L.; Lo, Y. S. Highly Efficient Quantum-Dot-Sensitized Solar Cell Based on Co-Sensitization of CdS/CdSe. *Adv. Funct. Mater.* **2009**, *19*, 604−609.

(27) Tisdale, W. A.; Williams, K. J.; Timp, B. A.; Norris, D. J.; Aydil, E. S.; Zhu, X. Y. Hot-Electron Transfer from Semiconductor Nanocrystals. *Science* **2010**, *328*, 1543−1547.

(28) Beard, M. C. Multiple Exciton Generation in Semiconductor Quantum Dots. *J. Phys. Chem. Lett.* **2011**, *2*, 1282−1288.

(29) Peumans, P.; Yakimov, A.; Forrest, S. R. Small Molecular Weight Organic Thin-Film Photodetectors and Solar Cells. *J. Appl. Phys.* **2003**, *93*, 3693−3723.

DOI: 10.1021/acs.jpcc.5b08131
J. Phys. Chem. C 2016, 120, 15657−15665

(30) Kim, S.; Lee, J. K.; Kang, S. O.; Ko, J.; Yum, J. H.; Fantacci, S.; De Angelis, F.; Di Censo, D.; Nazeeruddin, M. K.; Gratzel, M. Molecular Engineering of Organic Sensitizers for Solar Cell Applications. *J. Am. Chem. Soc.* **2006**, *128*, 16701−16707.
(31) Ameri, T.; Dennler, G.; Lungenschmied, C.; Brabec, C. J. Organic Tandem Solar Cells: A Review. *Energy Environ. Sci.* **2009**, *2*, 347−363.
(32) Choi, H.; Nicolaescu, R.; Paek, S.; Ko, J.; Kamat, P. V. Supersensitization of CdS Quantum Dots with a Near-Infrared Organic Dye: Toward the Design of Panchromatic Hybrid-Sensitized Solar Cells. *ACS Nano* **2011**, *5*, 9238−9245.
(33) Ji, G. Q.; Liu, Z. Q.; Guan, D. B.; Yang, Y. T. Ag_2S Quantum Dots and N_3 Dye Co-sensitized TiO_2 Nanotube Arrays for a Solar Cell. *Appl. Surf. Sci.* **2013**, *282*, 695−699.
(34) Lelii, C.; Bawendi, M. G.; Biagini, P.; Chen, P. Y.; Crucianelli, M.; D'Arcy, J. M.; De Angelis, F.; Hammond, P. T.; Po, R. Enhanced Photovoltaic Performance with Co-sensitization of Quantum Dots and an Organic Dye in Dye-Sensitized Solar Cells. *J. Mater. Chem. A* **2014**, *2*, 18375−18382.
(35) Meng, K.; Surolia, P. K.; Byrne, O.; Thampi, K. R. Quantum Dot and Quantum Dot-Dye Co-sensitized Solar Cells Containing Organic Thiolate-Disulfide Redox Electrolyte. *J. Power Sources* **2015**, *275*, 681−687.
(36) Shan, Y.; Xu, J. J.; Chen, H. Y. Distance-Dependent Quenching and Enhancing of Electrochemiluminescence from a CdS:Mn Nanocrystal Film by Au Nanoparticles for Highly Sensitive Detection of DNA. *Chem. Commun.* **2009**, 905−907.
(37) Pu, Y. C.; Wang, G.; Chang, K. D.; Ling, Y.; Lin, Y. K.; Fitzmorris, B. C.; Liu, C. M.; Lu, X.; Tong, Y.; Zhang, J. Z.; et al. Au Nanostructure-Decorated TiO_2 Nanowires Exhibiting Photoactivity Across Entire UV-visible Region for Photoelectrochemical Water Splitting. *Nano Lett.* **2013**, *13*, 3817−3823.
(38) Pradhan, N.; Sarma, D. D. Advances in Light-Emitting Doped Semiconductor Nanocrystals. *J. Phys. Chem. Lett.* **2011**, *2*, 2818−2826.
(39) Catchpole, K. R.; Polman, A. Design Principles for Particle Plasmon Enhanced Solar Cells. *Appl. Phys. Lett.* **2008**, *93*, 191113.
(40) Zarazua, I.; De la Rosa, E.; Lopez-Luke, T.; Reyes-Gomez, J.; Ruiz, S.; Chavez, C. A.; Zhang, J. Z. Photovoltaic Conversion Enhancement of CdSe Quantum Dot-Sensitized TiO_2 Decorated with Au Nanoparticles and P3OT. *J. Phys. Chem. C* **2011**, *115*, 23209−23220.
(41) Kuang, D. B.; Ito, S.; Wenger, B.; Klein, C.; Moser, J. E.; Humphry-Baker, R.; Zakeeruddin, S. M.; Gratzel, M. High Molar Extinction Coefficient Heteroleptic Ruthenium Complexes for Thin Film Dye-Sensitized Solar Cells. *J. Am. Chem. Soc.* **2006**, *128*, 4146−4154.
(42) Santra, P. K.; Kamat, P. V. Mn-Doped Quantum Dot Sensitized Solar Cells: A Strategy to Boost Efficiency over 5%. *J. Am. Chem. Soc.* **2012**, *134*, 2508−2511.
(43) Nag, A.; Chakraborty, S.; Sarma, D. D. To Dope Mn^{2+} in a Semiconducting Nanocrystal. *J. Am. Chem. Soc.* **2008**, *130*, 10605−10611.
(44) Subramanian, V.; Wolf, E.; Kamat, P. V. Semiconducto-Metal Composite Nanostructures. To What Extent Do Metal Nanoparticles Improve the Photocatalytic Activity of TiO_2 Films? *J. Phys. Chem. B* **2001**, *105*, 11439−11446.
(45) Liu, L. P.; Wang, G. M.; Li, Y.; Li, Y. D.; Zhang, J. Z. CdSe Quantum Dot-Sensitized Au/TiO_2 Hybrid Mesoporous Films and Their Enhanced Photoelectrochemical Performance. *Nano Res.* **2011**, *4*, 249−258.
(46) Zhang, X. R.; Zhao, Y. Q.; Li, S. G.; Zhang, S. S. Photoelectrochemical Biosensor for Detection of Adenosine Triphosphate in the Extracts of Cancer Cells. *Chem. Commun.* **2010**, *46*, 9173−9175.
(47) Sanghavi, B. J.; Sitaula, S.; Griep, M. H.; Karna, S. P.; Ali, M. F.; Swami, N. S. Real-Time Electrochemical Monitoring of Adenosine Triphosphate in the Picomolar to Micromolar Range Using Graphene-Modified Electrodes. *Anal. Chem.* **2013**, *85*, 8158−8165.
(48) Bu, N. N.; Gao, A.; He, X. W.; Yin, X. B. Electrochemiluminescent Biosensor of ATP Using Tetrahedron Structured DNA and a Functional Oligonucleotide for $Ru(phen)_3^{2+}$ Intercalation and Target Identification. *Biosens. Bioelectron.* **2013**, *43*, 200−204.
(49) Guo, Y.; Sun, X.; Yang, G.; Liu, J. Ultrasensitive Detection of ATP Based on ATP Regeneration Amplification and Its Application in Cell Homogenate and Human Serum. *Chem. Commun.* **2014**, *50*, 7659−7662.
(50) Lin, C.; Cai, Z.; Wang, Y.; Zhu, Z.; Yang, C. J.; Chen, X. Label-Free Fluorescence Strategy for Sensitive Detection of Adenosine Triphosphate Using a Loop DNA Probe with Low Background Noise. *Anal. Chem.* **2014**, *86*, 6758−6762.

DOI: 10.1021/acs.jpcc.5b08131
J. Phys. Chem. C 2016, 120, 15657−15665